10-2017

Quantum diffusion of electromagnetic fields of ultrarelativistic spin-half particles

Balthazar Peroutka
Iowa State University, peroutka@iastate.edu

Kirill Tuchin
Iowa State University, tuchin@iastate.edu

Quantum diffusion of electromagnetic fields of ultrarelativistic spin-half particles

Abstract

We compute electromagnetic fields created by a relativistic charged spin-half particle in empty space at distances comparable to the particle Compton wavelength. The particle is described as a wave packet evolving according to the Dirac equation. It produces the electromagnetic field that is essentially different from the Coulomb field due to the quantum diffusion effect.

Keywords

Electromagnetic field, Heavy-ion collisions

Disciplines

Nuclear | Physics

Comments

This is a manuscript of an article published as Peroutka, Balthazar, and Kirill Tuchin. "Quantum diffusion of electromagnetic fields of ultrarelativistic spin-half particles." *Nuclear Physics A* 966 (2017): 64-72. DOI: 10.1016/j.nuclphysa.2017.05.104. Posted with permission.

Quantum diffusion of electromagnetic fields of ultrarelativistic spin-half particles

Balthazar Peroutka[1] and Kirill Tuchin[1]

[1]*Department of Physics and Astronomy, Iowa State University, Ames, Iowa, 50011, USA*

(Dated: February 12, 2018)

We compute electromagnetic fields created by a relativistic charged spin-half particle in empty space at distances comparable to the particle Compton wavelength. The particle is described as a wave packet evolving according to the Dirac equation. It produces the electromagnetic field that is essentially different from the Coulomb field due to the quantum diffusion effect.

I. INTRODUCTION

It has been known for a while that very intense electromagnetic fields are created in ultra-relativistic hadronic and nuclear collisions [1–5]. However, no convincing experimental evidence of their impact on the scattering dynamics has been observed. In recent years, a renewed interest to this subject was motivated by the relativistic heavy-ion collision experiments. The electromagnetic fields are intense enough to modify the properties of the nuclear matter produced in these collisions. In order to evaluate the impact of these fields on the nuclear matter, it is crucial to know their space-time structure. In [6–12] production of the electromagnetic fields was studied using the hadron transport models, neglecting the nuclear medium electric and magnetic response and flow. In [9, 11, 12] it was pointed out that the quantum nature of the nucleus wave function gives rise to strong field fluctuation, so that even in central collisions the r.m.s. does not vanish. In [13–16] it is argued that due to the finite electric conductivity of nuclear matter, the lifetime of the electromagnetic field is significantly longer than in vacuum. Anomalous transport can also affect the field producing oscillations [17–19] and even forcing the field into the topologically non-trivial configurations [20–25]. The electromagnetic field in the nuclear medium, unlike that in vacuum, strongly depends on the initial conditions [26]. The nuclear medium produced in relativistic heavy-ion collisions is well described by the relativistic hydrodynamics. Relativistic magneto-hydrodynamic calculations were done in [27–29] in the ideal limit (infinite electrical conductivity).

In a recent publication [30] we argued that one can treat the sources of the electromagnetic field, i.e. the valence quarks, neither as point particles (classical limit) nor as plane waves, which have infinite spatial extent. This is because the interaction range, the quark wave function size and the dimensions of the produced nuclear matter have similar extent. As the first step towards understanding the quantum dynamics of the electromagnetic field sources, in [30] we modeled valence quarks as spinless Gaussian wave packets. Solving the Klein-Gordon equation we computed the charge and current densities and the resulting electromagnetic fields in vacuum. In the present work we extend our approach to compute the spin contribution to the electromagnetic field. As in [30] we start with the initial Gaussian wave packet and evolve it in time according to the Dirac equation. At this point we completely neglect the medium effects as our goal is to study the effect of quantum diffusion of the quark wave function. This way our calculation is applicable to any hadronic and nuclear collisions.

Before we proceed to the description of our calculation, it is worthwhile to set the notations, definitions and normalizations. The wave function of a spin-half particle can be expanded in a complete set of the momentum and helicity eigenstates:

$$\Psi(\boldsymbol{r},t) = \frac{1}{\sqrt{2}}\sum_{\lambda}\int \frac{d^3k}{(2\pi)^{3/2}} e^{i\boldsymbol{k}\cdot\boldsymbol{r}} e^{-i\varepsilon_k t}\psi_{\boldsymbol{k}}(0) u_{\boldsymbol{k}\lambda}\,, \tag{1}$$

where $\varepsilon_k = \sqrt{m^2+k^2}$. The four-component bispinor $u_{\boldsymbol{k}\lambda}$ is the momentum and helicity eigenstate normalized as

$$u^{\dagger}_{\boldsymbol{k}\lambda} u_{\boldsymbol{k}\lambda'} = \delta_{\lambda\lambda'}\,. \tag{2}$$

$\psi_{\boldsymbol{k}}(0)$ is the momentum wave function at $t=0$, normalized as

$$\int |\psi_{\boldsymbol{k}}(0)|^2 d^3k = 1\,. \tag{3}$$

With these conventions

$$\int \Psi^{\dagger}(\boldsymbol{r},t)\Psi(\boldsymbol{r},t) d^3r = 1\,. \tag{4}$$

Solutions of the Dirac equation with given momentum $\boldsymbol{k}$ and helicity $\lambda = \pm$ normalized by (2) are

$$u_{\boldsymbol{k}+} = \sqrt{\frac{\varepsilon_k+m}{2\varepsilon_k}}\begin{pmatrix}\chi_+ \\ \frac{\boldsymbol{\sigma}\cdot\boldsymbol{k}}{\varepsilon_k+m}\chi_+\end{pmatrix}\,, \quad u_{\boldsymbol{k}-} = \sqrt{\frac{\varepsilon_k+m}{2\varepsilon_k}}\begin{pmatrix}\chi_- \\ \frac{\boldsymbol{\sigma}\cdot\boldsymbol{k}}{\varepsilon_k+m}\chi_-\end{pmatrix}\,, \tag{5}$$

where the two-component spinors $\chi_\pm$ are helicity eigenstates.

II. REST FRAME

In the rest frame, although the particle momentum vanishes, the momentum of the Fourier components in (1) is finite, which is the reason for the wave function diffusion. Although the particle spin projection on any axis is conserved, only spin projection on the momentum direction is conserved for states with given momentum. This is why the helicity eigenstates are the correct choice of the spin basis.

Taking the direction of observation to be z-axis, i.e. $\boldsymbol{r} = r\hat{\boldsymbol{z}}$ and describing the momentum direction by the polar and azimuthal angles θ and ϕ we write the helicity eigenstates

$$\chi_+ = \begin{pmatrix} \cos\frac{\theta}{2} \\ \sin\frac{\theta}{2}e^{i\phi} \end{pmatrix}, \quad \chi_- = \begin{pmatrix} \sin\frac{\theta}{2} \\ -\cos\frac{\theta}{2}e^{i\phi} \end{pmatrix}. \tag{6}$$

Using these in (5) yields

$$u_{\boldsymbol{k}+} = \sqrt{\frac{\varepsilon_k + m}{2\varepsilon_k}} \begin{pmatrix} \cos\frac{\theta}{2} \\ \sin\frac{\theta}{2}e^{i\phi} \\ \frac{k}{\varepsilon_k+m}\cos\frac{\theta}{2} \\ \frac{k}{\varepsilon_k+m}\sin\frac{\theta}{2}e^{i\phi} \end{pmatrix}, \quad u_{\boldsymbol{k}-} = \sqrt{\frac{\varepsilon_k + m}{2\varepsilon_k}} \begin{pmatrix} \sin\frac{\theta}{2} \\ -\cos\frac{\theta}{2}e^{i\phi} \\ -\frac{k}{\varepsilon_k+m}\sin\frac{\theta}{2} \\ \frac{k}{\varepsilon_k+m}\cos\frac{\theta}{2}e^{i\phi} \end{pmatrix}, \tag{7}$$

Plugging (7) into (1) yields, after integration over the momentum directions (keeping in mind that $\boldsymbol{k}\cdot\boldsymbol{r} = kr\cos\theta$), the wave function in the rest frame

$$\Psi(\boldsymbol{r},t) = \frac{1}{2\sqrt{\pi}}\int_0^\infty dk k^2 e^{-i\varepsilon_k t}\psi_{\boldsymbol{k}}(0)\sqrt{\frac{\varepsilon_k + m}{2\varepsilon_k}} \begin{pmatrix} f(kr) \\ 0 \\ \frac{ik}{\varepsilon_k+m}g(kr) \\ 0 \end{pmatrix} \tag{8}$$

where

$$\begin{aligned} f(z) &= \frac{1}{\sqrt{2}}\int_{-1}^{1}(\sqrt{1+x}+\sqrt{1-x})e^{izx}dx \\ &= \frac{\sqrt{\pi}}{z^{3/2}}\left\{\sqrt{\frac{4z}{\pi}}\sin(z) - \cos(z)S\left(\sqrt{\frac{4z}{\pi}}\right) + \sin(z)C\left(\sqrt{\frac{4z}{\pi}}\right)\right\}, \end{aligned} \tag{9}$$

$$\begin{aligned} g(z) &= \frac{1}{i\sqrt{2}}\int_{-1}^{1}(\sqrt{1+x}-\sqrt{1-x})e^{izx}dx \\ &= \frac{\sqrt{\pi}}{z^{3/2}}\left\{-\sqrt{\frac{4z}{\pi}}\cos(z) + \sin(z)S\left(\sqrt{\frac{4z}{\pi}}\right) + \cos(z)C\left(\sqrt{\frac{4z}{\pi}}\right)\right\}. \end{aligned} \tag{10}$$

where C and S are the Fresnel integrals related to the error function:

$$C(z) + iS(z) = \frac{1+i}{2}\operatorname{erf}\left[\frac{\sqrt{\pi}}{2}(1-i)z\right]. \tag{11}$$

The corresponding charge and current densities are obtained using

$$\rho = e\Psi^\dagger\Psi, \quad \boldsymbol{j} = e\Psi^\dagger\boldsymbol{\alpha}\Psi. \tag{12}$$

The resulting ρ and $\boldsymbol{j}$ are spherically symmetric. In particular $\boldsymbol{j}$ is directed along the z-axis, which coincides with the direction of $\boldsymbol{r}$ in our coordinate system.

$$\rho(\boldsymbol{r},t) = \frac{e}{4\pi}\int_0^\infty dk k^2 \psi_{\boldsymbol{k}}(0)\sqrt{\frac{\varepsilon_k+m}{2\varepsilon_k}}\int_0^\infty dl l^2 \psi_{\boldsymbol{l}}(0)\sqrt{\frac{\varepsilon_l+m}{2\varepsilon_l}} \times\left\{f(kr)f(lr)+\frac{k}{\varepsilon_k+m}\frac{l}{\varepsilon_l+m}g(kr)g(lr)\right\}\cos[(\varepsilon_k-\varepsilon_l)t]\,. \tag{13}$$

$$\boldsymbol{j}(\boldsymbol{r},t) = \hat{\boldsymbol{r}}\frac{e}{4\pi}\int_0^\infty dk k^2 \psi_{\boldsymbol{k}}(0)\sqrt{\frac{\varepsilon_k+m}{2\varepsilon_k}}\int_0^\infty dl l^2 \psi_{\boldsymbol{l}}(0)\sqrt{\frac{\varepsilon_l+m}{2\varepsilon_l}} \times\left\{f(kr)\frac{l}{\varepsilon_l+m}g(lr)-g(kr)\frac{k}{\varepsilon_k+m}f(lr)\right\}\sin[(\varepsilon_l-\varepsilon_k)t]\,. \tag{14}$$

Given the charge and current densities, the electric field can be computed as

$$\boldsymbol{E}(\boldsymbol{r},t) = \int\left\{\frac{\rho(\boldsymbol{r}',t')\boldsymbol{R}}{R^3}+\frac{\boldsymbol{R}}{R^2}\frac{\partial\rho(\boldsymbol{r}',t')}{\partial t'}-\frac{1}{R}\frac{\partial\boldsymbol{j}(\boldsymbol{r}',t')}{\partial t'}\right\}d^3r'\,, \tag{15}$$

where $t'=t-|\boldsymbol{r}-\boldsymbol{r}'|$ is the retarded time and $\boldsymbol{R}=\boldsymbol{r}-\boldsymbol{r}'$. The only non-vanishing component of the electromagnetic field in the rest frame is the radial component of the electric field E:

$$\boldsymbol{E}(\boldsymbol{r},t) = E(r,t)\hat{\boldsymbol{r}}\,, \qquad \boldsymbol{B}(\boldsymbol{r},t)=0\,. \tag{16}$$

We emphasize, that although the entire discussion of this section deals with a charged point particle at rest, its electromagnetic field $\boldsymbol{E}(\boldsymbol{r},t)$ is different from the Coulomb field $e\boldsymbol{r}/4\pi r^3$ due to the quantum evolution of the particle wave function.

III. CONVECTIVE AND SPIN CURRENTS

It is instructive to separate the convective and spin contributions (marked below by the subscripts c and s respectively). Using the Gordon identity

$$\bar\Psi_2\gamma^\mu\Psi_1 = \frac{1}{2m}\left[\bar\Psi_2 i\partial^\mu\Psi_1-(i\partial^\mu\bar\Psi_2)\Psi_1\right]-\frac{1}{2m}i\partial_\nu(\bar\Psi_2\sigma^{\mu\nu}\Psi_1) \tag{17}$$

we can write the charge and current densities (12) as

$$\rho=\rho_c+\rho_s\,, \qquad \boldsymbol{j}=\boldsymbol{j}_c+\boldsymbol{j}_s\,, \tag{18}$$

where

$$\rho_c=\frac{ie}{2m}(\bar\Psi\dot\Psi-\dot{\bar\Psi}\Psi)\,, \qquad \boldsymbol{j}_c=\frac{ie}{2m}\left[(\boldsymbol{\nabla}\bar\Psi)\Psi-\bar\Psi(\boldsymbol{\nabla}\Psi)\right]\,, \tag{19}$$

$$\rho_s=-\frac{e}{2m}\boldsymbol{\nabla}\cdot(\Psi^\dagger\boldsymbol{\Sigma}\Psi)\,, \qquad \boldsymbol{j}_s=\frac{e}{2m}\partial_t(\Psi^\dagger\boldsymbol{\Sigma}\Psi)-\frac{ie}{2m}\boldsymbol{\nabla}\times(\Psi^\dagger\gamma_0\boldsymbol{\Sigma}\Psi)\,. \tag{20}$$

Explicit expressions for the convective charge and current densities read

$$\rho_c(\boldsymbol{r},t) = \frac{e}{8\pi m}\int_0^\infty dk k^2\psi_{\boldsymbol{k}}(0)\sqrt{\frac{\varepsilon_k+m}{2\varepsilon_k}}\int_0^\infty dl l^2\psi_{\boldsymbol{l}}(0)\sqrt{\frac{\varepsilon_l+m}{2\varepsilon_l}}$$

$$\times(\varepsilon_k+\varepsilon_l)\left\{f(kr)f(lr)+\frac{k}{\varepsilon_k+m}\frac{l}{\varepsilon_l+m}g(kr)g(lr)\right\}\cos[(\varepsilon_k-\varepsilon_l)t]\,. \quad (21)$$

$$\boldsymbol{j}_c(\boldsymbol{r},t) = \hat{\boldsymbol{r}}\frac{e}{8\pi m}\int_0^\infty dk k^2\psi_{\boldsymbol{k}}(0)\sqrt{\frac{\varepsilon_k+m}{2\varepsilon_k}}\int_0^\infty dl l^2\psi_{\boldsymbol{l}}(0)\sqrt{\frac{\varepsilon_l+m}{2\varepsilon_l}}\sin[(\varepsilon_l-\varepsilon_k)t]$$

$$\times\left\{lf(kr)f'(lr)-kf'(kr)f(lr)+\frac{l}{\varepsilon_l+m}\frac{k}{\varepsilon_k+m}\left[lg(kr)g'(lr)-kg'(kr)g(lr)\right]\right\}\,. \quad (22)$$

Here the integrals

$$f'(z) = -\frac{1}{\sqrt{2}}\int_{-1}^{1}(\sqrt{1+x}+\sqrt{1-x})x\sin(zx)dx\,, \quad (23)$$

$$g'(z) = \frac{1}{\sqrt{2}}\int_{-1}^{1}(\sqrt{1+x}-\sqrt{1-x})x\cos(zx)dx \quad (24)$$

can be expressed in terms of the Fresnel integrals (11). The corresponding field is computed using (15).

IV. LAB FRAME

In the Lab frame moving with constant velocity $-v\hat{\boldsymbol{z}}$ with respect to the rest frame, the electric charge moves with velocity $v\hat{\boldsymbol{z}}$. In contrast to the previous sections, in this and the next sections, all quantities pertaining to the rest frame are denoted by the subscript 0, whereas those pertaining to the Lab frame bear no such subscript. The Lorentz transformations relating the coordinates and the fields in the two frames are

$$\boldsymbol{r}_{\perp 0} = \boldsymbol{r}_\perp\,, \qquad z_0 = \gamma(z-vt)\,, \quad (25)$$

$$E_{z0} = E_z\,, \qquad B_{z0} = B_z\,, \quad (26)$$

$$\boldsymbol{E}_{\perp 0} = \gamma(\boldsymbol{E}_\perp + v\hat{\boldsymbol{z}}\times\boldsymbol{B}_\perp)\,, \qquad \boldsymbol{B}_{\perp 0} = \gamma(\boldsymbol{B}_\perp - v\hat{\boldsymbol{z}}\times\boldsymbol{E}_\perp)\,. \quad (27)$$

Here $\gamma^{-1} = \sqrt{1-v^2}$ and $\boldsymbol{r}_\perp\cdot\hat{\boldsymbol{z}} = 0$. Thus, the electric field (16) in the Lab frame transforms into

$$E_z = E_{z0}\,, \qquad B_z = 0\,, \quad (28)$$

$$\boldsymbol{E}_\perp = \gamma\boldsymbol{E}_{\perp 0}\,, \qquad \boldsymbol{B}_\perp = \gamma v\hat{\boldsymbol{z}}\times\boldsymbol{E}_{\perp 0}\,. \quad (29)$$

Using the cylindrical coordinates one can write

$$\boldsymbol{E} = E_\perp\hat{\boldsymbol{b}} + E_z\hat{\boldsymbol{z}}\,, \qquad \boldsymbol{B} = B\hat{\boldsymbol{\phi}}\,, \quad (30)$$

where

$$E_z(\boldsymbol{r},t) = E_0\left(\sqrt{b^2+\gamma^2(z-vt)^2}, \gamma(t-vz)\right)\frac{\gamma(z-vt)}{\sqrt{b^2+\gamma^2(z-vt)^2}}\,, \tag{31}$$

$$B(\boldsymbol{r},t) = E_0\left(\sqrt{b^2+\gamma^2(z-vt)^2}, \gamma(t-vz)\right)\frac{v\gamma b}{\sqrt{b^2+\gamma^2(z-vt)^2}}\,, \tag{32}$$

and $E_\perp = B/v$. $E_0(r_0,t_0)$ is the magnitude of the electric field in the rest frame. Impact parameter b is a distance from the moving charge in the transverse direction.

V. RESULTS

To compute the electromagnetic field created by a relativistic wave packet, one needs to specify the initial wave function. We adopted a Gaussian distribution

$$\psi_{\boldsymbol{k}}(0) = \frac{a^{3/2}}{\pi^{3/4}}e^{-a^2k^2/2}\,. \tag{33}$$

Its width in the coordinate space is fixed at $a = 1$ fm reflecting the strong interactions range. We also assumed that the momentum wave function is independent of λ, i.e. it is the same for all spin states. Other parameters used in our numerical calculations were the valence quark mass $m = 0.3$ GeV, electric charge e (we omit the quark charges 2/3 and -1/3) and the boost factor $\gamma = 100$.

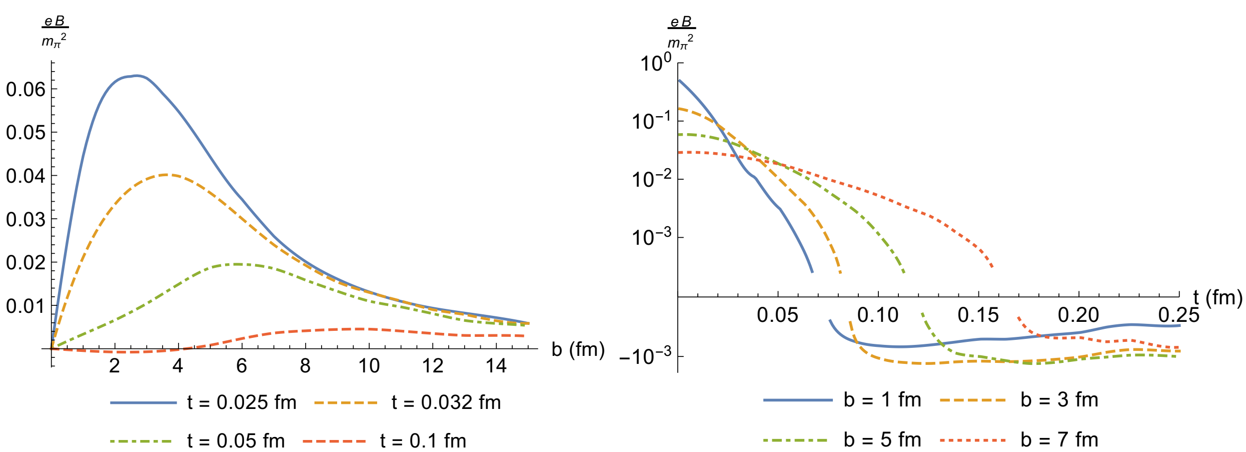

FIG. 1: Magnetic field generated by a wave packet of width $a = 1$ fm as a function of impact parameter b (left panel) and time t (right panel). Notice, that in the right panel, there is no discontinuity of the magnetic field, as might appear at first sight. It is an artifact of the logarithmic scale on the vertical axis, see Fig. 3.

The results of our calculations are exhibited in Fig. 1-Fig. 3. Shown in Fig. 1 is the dependence of the magnetic field on time t (left panel) and distance b (right panel). On the left panel notice

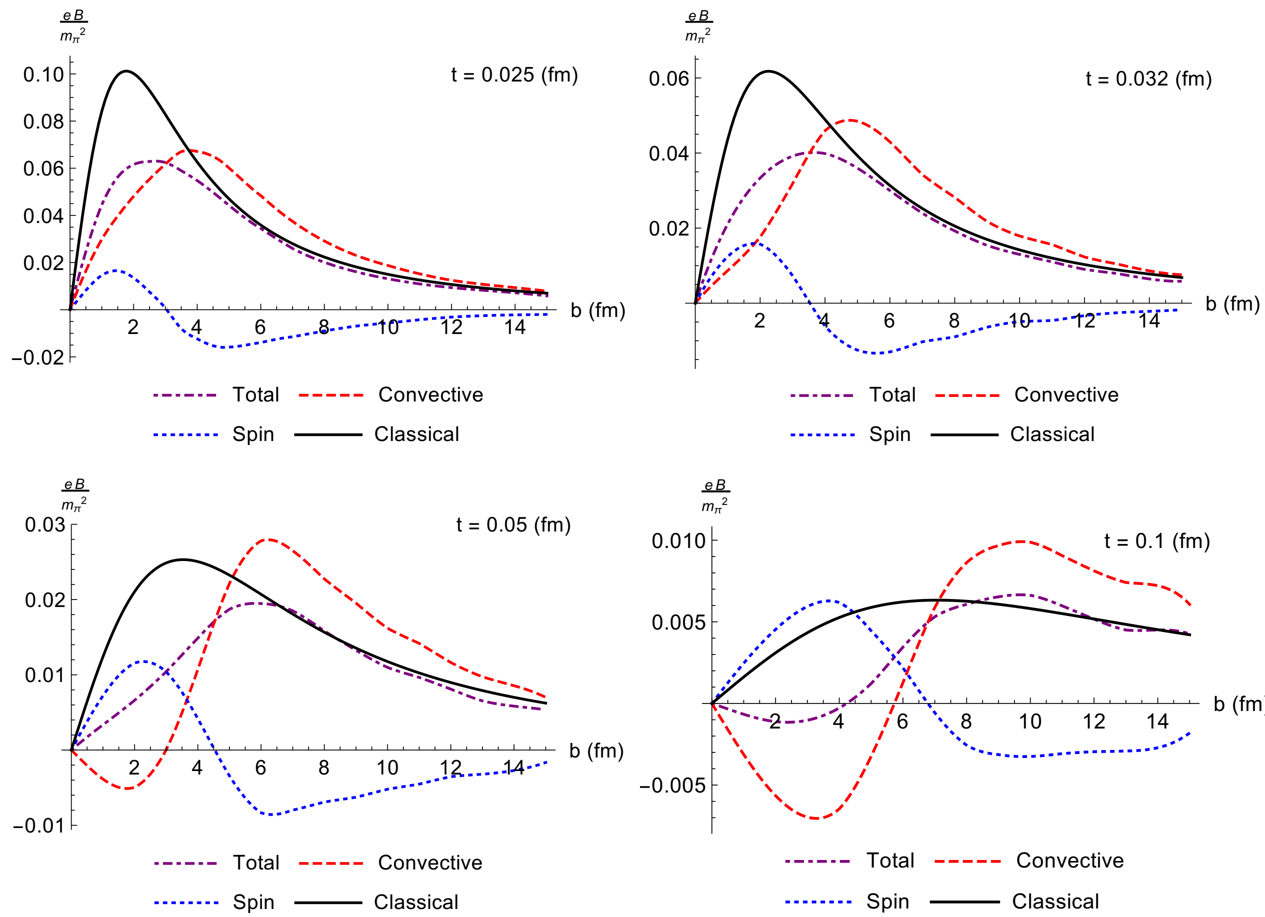

FIG. 2: Dependence of magnetic field on the transverse distance from the charge b at different times.

that at later time the magnetic field changes sign. We have observed this effect before for a scalar particle [30], where it is, in fact, much more prominent. We will add a few more comments about the sign flip later in this section.

In Fig. 2 we plot each of the lines shown in Fig. 1 (left panel) separately along with its convective and spin components. Also plotted is the corresponding classical (boosted Coulomb) field for comparison. At large b, the classical (i.e. point) and quantum (i.e. wave packet) sources induce the same field as expected. While the convective current contributes to the monopole term falling off as $1/b^2$ at large b, the leading spin current contribution starts with the dipole term which falls off as $1/b^3$. At later times, due to the quantum diffusion, the deviation from the classical field is observed in a wider range of distances.

In Fig. 3 we plot each of the lines shown in Fig. 1 (right panel) separately along with its convective and spin components as well as the classical field. In order to better demonstrate the sign flip dynamics we use the linear scale for the vertical axis. It is seen that while the convective

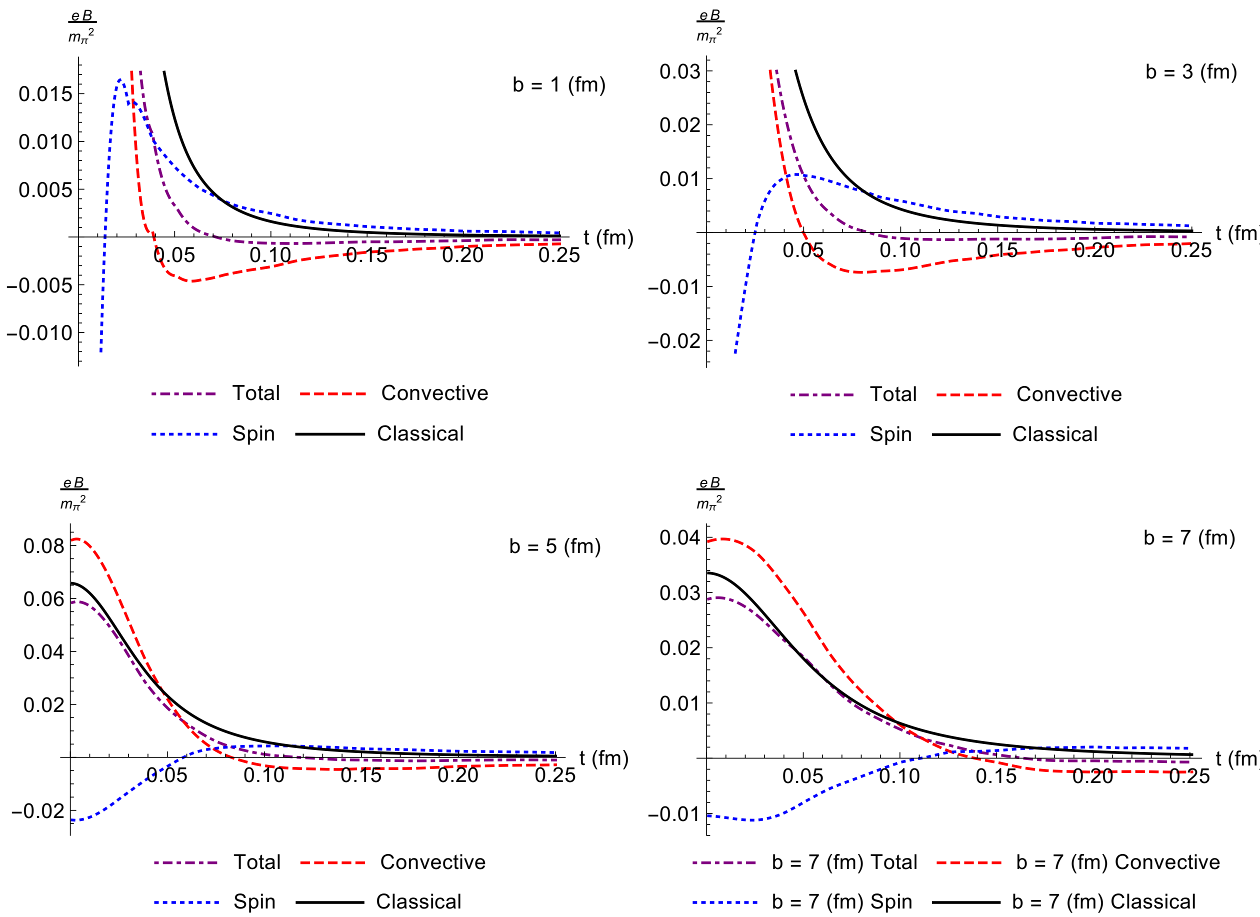

FIG. 3: Dependence of magnetic field on time t at different transverse distances b from the charge.

part of the magnetic field changes its sign from positive to negative, the spin part changes its sign from negative to positive at about the same time. This makes the sign flip effect for the magnetic field generated by spin-1/2 particle less pronounced than for the field generated by a scalar particle (computed in [30]). The origin of the spin flip can be traced back to (15) in which the last two terms are proportional to the rate of decrease of charge density and the corresponding increase of the current density due to the quantum diffusion of the wave packet in the outward radial direction.

VI. CONCLUSIONS

We computed the magnetic field created by a single valence quark, which is represented by a wave packet satisfying the Dirac equation and moving in free space with relativistic velocity. We observed that the classical description of the valence quarks as point-particles is not accurate for calculations of the electromagnetic field in hadron and/or nuclear collisions as it breaks down at distances as large as 6 fm at $\gamma = 100$. Moreover it misses an important spin-flip effect that occurs due to the quantum diffusion of the wave packet.

This paper is a step towards our ultimate goal of determining the structure and dynamics of electromagnetic fields created in relativistic hadron and nuclear collisions, and in particular, in heavy-ion collisions. In the forthcoming publication, we intend to study the effect of the conducting medium on the electromagnetic field created by quantum sources.

Acknowledgments

This work was supported in part by the U.S. Department of Energy under Grant No. DE-FG02-87ER40371.

[1] W. Greiner, B. Muller and J. Rafelski, "Quantum Electrodynamics Of Strong Fields," Berlin, Germany: Springer (1985) 594 P. (Texts and Monographs In Physics)

[2] J. Rafelski and B. Muller, "Magnetic Splitting of Quasimolecular Electronic States in Strong Fields," Phys. Rev. Lett. **36**, 517 (1976).

[3] J. Ambjorn and P. Olesen, "On Electroweak Magnetism," Nucl. Phys. B **315**, 606 (1989).

[4] J. Ambjorn and P. Olesen, "W condensate formation in high-energy collisions," Phys. Lett. B **257**, 201 (1991).

[5] P. Olesen, "W condensation at the LHC?," arXiv:1207.7045 [hep-ph].

[6] D. E. Kharzeev, L. D. McLerran and H. J. Warringa, "The effects of topological charge change in heavy ion collisions: 'Event by event P and CP violation'," Nucl. Phys. A **803**, 227 (2008).

[7] V. Skokov, A. Y. Illarionov and V. Toneev, "Estimate of the magnetic field strength in heavy-ion collisions," Int. J. Mod. Phys. A **24**, 5925 (2009)

[8] V. Voronyuk, V. D. Toneev, W. Cassing, E. L. Bratkovskaya, V. P. Konchakovski and S. A. Voloshin, "(Electro-)Magnetic field evolution in relativistic heavy-ion collisions," Phys. Rev. C **83**, 054911 (2011)

[9] J. Bloczynski, X. G. Huang, X. Zhang and J. Liao, "Azimuthally fluctuating magnetic field and its impacts on observables in heavy-ion collisions," Phys. Lett. B **718**, 1529 (2013)

[10] L. Ou and B. A. Li, "Magnetic effects in heavy-ion collisions at intermediate energies," Phys. Rev. C **84**, 064605 (2011)

[11] W. T. Deng and X. G. Huang, "Event-by-event generation of electromagnetic fields in heavy-ion collisions," Phys. Rev. C **85**, 044907 (2012)

[12] A. Bzdak and V. Skokov, "Event-by-event fluctuations of magnetic and electric fields in heavy ion collisions," Phys. Lett. B **710**, 171 (2012)

[13] K. Tuchin, "Synchrotron radiation by fast fermions in heavy-ion collisions," Phys. Rev. C **82**, 034904 (2010) [Erratum-ibid. C **83**, 039903 (2011)].

[14] B. G. Zakharov, “Electromagnetic response of quark-gluon plasma in heavy-ion collisions,” Phys. Lett. B **737**, 262 (2014)

[15] K. Tuchin, “Time and space dependence of the electromagnetic field in relativistic heavy-ion collisions,” Phys. Rev. C **88**, no. 2, 024911 (2013)

[16] K. Tuchin, “Particle production in strong electromagnetic fields in relativistic heavy-ion collisions,” Adv. High Energy Phys. **2013**, 490495 (2013)

[17] K. Tuchin, “Electromagnetic field and the chiral magnetic effect in the quark-gluon plasma,” Phys. Rev. C **91**, no. 6, 064902 (2015)

[18] C. Manuel and J. M. Torres-Rincon, “Dynamical evolution of the chiral magnetic effect: Applications to the quark-gluon plasma,” Phys. Rev. D **92**, no. 7, 074018 (2015)

[19] H. Li, X. l. Sheng and Q. Wang, “Electromagnetic fields with electric and chiral magnetic conductivities in heavy ion collisions,” Phys. Rev. C **94**, no. 4, 044903 (2016)

[20] K. Tuchin, “Excitation of Chandrasekhar-Kendall photons in quark gluon plasma by propagating ultrarelativistic quarks,” Phys. Rev. C **93**, no. 5, 054903 (2016)

[21] K. Tuchin, “Spontaneous topological transitions of electromagnetic fields in spatially inhomogeneous CP-odd domains,” Phys. Rev. C **94**, no. 6, 064909 (2016)

[22] Y. Hirono, D. E. Kharzeev and Y. Yin, “Quantized chiral magnetic current from reconnections of magnetic flux,” Phys. Rev. Lett. **117**, no. 17, 172301 (2016)

[23] Y. Hirono, D. Kharzeev and Y. Yin, “Self-similar inverse cascade of magnetic helicity driven by the chiral anomaly,” Phys. Rev. D **92**, no. 12, 125031 (2015)

[24] X. l. Xia, H. Qin and Q. Wang, “Approach to Chandrasekhar-Kendall-Woltjer State in a Chiral Plasma,” Phys. Rev. D **94**, no. 5, 054042 (2016)

[25] Z. Qiu, G. Cao and X. G. Huang, “On electrodynamics of chiral matter,” Phys. Rev. D **95**, no. 3, 036002 (2017)

[26] K. Tuchin, “Initial value problem for magnetic fields in heavy ion collisions,” Phys. Rev. C **93**, no. 1, 014905 (2016)

[27] G. Inghirami, L. Del Zanna, A. Beraudo, M. H. Moghaddam, F. Becattini and M. Bleicher, “Numerical magneto-hydrodynamics for relativistic nuclear collisions,” Eur. Phys. J. C **76**, no. 12, 659 (2016)

[28] V. Roy, S. Pu, L. Rezzolla and D. Rischke, Phys. Lett. B **750**, 45 (2015)

[29] S. Pu, V. Roy, L. Rezzolla and D. H. Rischke, “Bjorken flow in one-dimensional relativistic magnetohydrodynamics with magnetization,” Phys. Rev. D **93**, no. 7, 074022 (2016)

[30] R. Holliday, R. McCarty, B. Peroutka and K. Tuchin, “Classical electromagnetic fields from quantum sources in heavy-ion collisions,” Nucl. Phys. A **957**, 406 (2017)